JACS
JOURNAL OF THE AMERICAN CHEMICAL SOCIETY
Communication
pubs.acs.org/JACS

Liposome–Gold Nanorod Hybrids for High-Resolution Visualization Deep in Tissues

Neus Lozano,[†] Wafa' T. Al-Jamal,[†] Adrian Taruttis,[‡] Nicolas Beziere,[‡] Neal C. Burton,[‡] Jeroen Van den Bossche,[†] Mariarosa Mazza,[†] Eva Herzog,[‡] Vasilis Ntziachristos,*[,‡] and Kostas Kostarelos*[,†]

[†]Nanomedicine Laboratory, Centre for Drug Delivery Research, UCL School of Pharmacy, University College London, 29-39 Brunswick Square, London WC1N 1AX, U.K.

[‡]Institute for Biological and Medical Imaging (IBMI), Helmholtz Zentrum Munich, Technical University Munich, Munich, Germany

Supporting Information

ABSTRACT: The design of liposome–nanoparticle hybrids offers a rich toolbox for the fabrication of multifunctional modalities. A self-assembled liposome–gold nanorod hybrid vesicular system that consists of lipid-bilayer-associated gold nanorods designed to allow deep tissue detection, therapy, and monitoring in living animals using multispectral optoacoustic tomography has been fabricated and characterized in vitro and in vivo.

There is a growing need for the engineering of novel probes to allow noninvasive, combinatory therapeutic–diagnostic applications. We have proposed that the design of liposome–nanoparticle hybrids can offer a rich toolbox for the fabrication of such multifunctional modalities.[1] Here we describe the previously unreported construction of a hybrid liposome–gold nanorod vesicular system that consists of cationic liposomes and gold nanorods (AuNRs) designed to allow deep tissue detection, therapy, and monitoring in living animals using multispectral optoacoustic tomography (MSOT).[2]

Liposomes consisting of the cationic lipid *N*-[1-(2,3-dioleoyloxy)propyl]-*N*,*N*,*N*-trimethylammonium methyl sulfate (DOTAP) and cholesterol (Chol) have been previously studied extensively as nonviral delivery vehicles for gene therapy both preclinically and in clinical trials.[3] On the other hand, the use of AuNRs is very promising for diagnostic purposes since the two differentiated surface plasmon bands of AuNRs offer powerful optical properties that allow in vivo deep tissue imaging.[4,5] In this work, double-labeled NIR-liposome–AuNR hybrids using NIR-797:DOPE–DOTAP:Chol liposomes and surface-functionalized 780 nm AuNRs (Ntracker 30-PM-780) were engineered by self-assembly using the lipid film hydration and sonication methodology. The near-IR (NIR) molecular probe NIR-797 was incorporated into the hybrid vesicles by covalently linking the organic dye to the lipid 1,2-dioleoyl-*sn*-glycero-3-phosphoethanolamine (DOPE) to label the liposome bilayer [see the Supporting Information (SI)]. The vesicle hybrids were characterized using a battery of techniques, including dynamic light scattering (DLS), ζ-potential measurements, transmission electron microscopy (TEM), atomic force microscopy (AFM), and UV–vis spectroscopy (Figure 1).

The physicochemical and structural properties of the NIR-liposome–AuNR hybrids were compared with those of NIR-liposomes. DLS showed that NIR-liposomes gave a rather wide, single-diameter distribution with a mean at approximately 200 nm, while the liposome–AuNR hybrids led to generally smaller vesicles with mean diameters between 100 and 120 nm (Figure 1a). That was thought to be due to the vesicle-stabilizing effect of the nanorods as they self-assembled around the lipid bilayer, which was supported by the reduction in ζ-potential obtained for the hybrid compared with plain liposomes (Figure 1b). The polydispersity index (PI) obtained for the hybrid system was broad as a result of background signal interference from the nonspherical AuNRs.

Further structural elucidation of the liposome–AuNR hybrid vesicles was attempted using TEM and AFM. TEM investigations showed that NIR-liposomes alone formed unilamellar vesicles with nonuniform diameters ranging from 100 to 200 nm, consistent with the size determination obtained by DLS (Figure 1c). In contrast, the liposome–AuNR hybrid vesicles formed more uniformly sized vesicles with diameters of about 100 nm. Most importantly, the TEM investigation of the interactions between the liposomes and the AuNRs revealed that the AuNRs associated almost exclusively with the vesicular lipid bilayer and localized at the periphery of the vesicles. The hybrid liposomes were further imaged using AFM operated in tapping mode. Figure 1d shows the amplitude, 3D image, and cross-section analysis of the height image, providing further information about the bilayer thickness. Cross-section analysis of the NIR-liposomes indicated a thickness of approximately 5 nm on the mica surface, as expected for plain liposomes. However, the incorporation of AuNRs increased the height of the objects from 5 to 15 nm, confirming the interaction between the lipid bilayers and the AuNRs. In addition, AFM images revealed homogeneous size distributions without evidence of vesicle aggregation. On the basis of column fractionation, DLS, and UV–vis characterization of the eluted fractions (Figure S1 in the SI), we determined that at least 75% of the AuNRs remained associated with vesicle hybrids at a theoretical mean approximation of one nanorod per four

Received: May 17, 2012
Published: August 1, 2012

   dx.doi.org/10.1021/ja304499q | *J. Am. Chem. Soc.* 2012, 134, 13256–13258

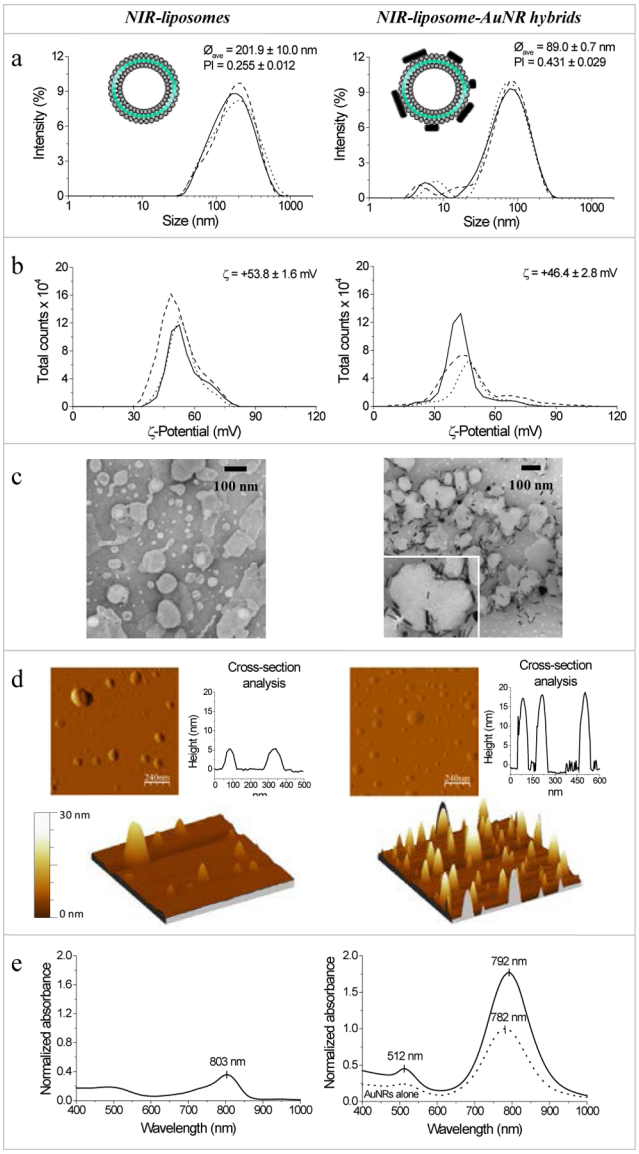

Figure 1. Physicochemical and structural characterization of NIR-liposomes and NIR-liposome–AuNR hybrids. (a) Schematic of the vesicle structures and DLS particle size distribution. (b) ζ-potential measurements. (c) TEM images. (d) AFM amplitude, 3D image, and cross-section analysis on mica. (e) UV–vis absorption spectra.

vesicles, which suggested the presence of liposomes alone within the hybrid vesicle sample.

To investigate whether electrostatic interactions between the lipid bilayer (cationic) and the AuNRs (PEG/methyl-coated) were responsible for the observed association and hybrid formation, NIR-liposomes were preformed in dextrose and then mixed with AuNRs. The physicochemical and structural characterization of this mixed system indicated no significant interactions between the AuNRs and the preformed liposomes (Figure S2). Therefore, the association between NIR-liposomes and AuNRs leading to the formation of hybrid vesicles can be attributed to different types of interactions (e.g., hydrophobic, self-assembly) between the lipid membranes and AuNRs. Further experimental work is needed to verify such a hypothesis and relate it with previously reported electrostatic interactions of AuNRs with preformed microgels[6,7] and silica particles.[8]

Figure 1e shows the absorbance spectra of both NIR-liposomes alone and the vesicle hybrids as a function of wavelength. The NIR-liposome spectrum presents an absorption band at 803 nm attributed to the excitation wavelength of the organic dye molecule NIR-797. On the other hand, the NIR-liposome–AuNR hybrids maintained the two characteristic surface plasmon bands from the AuNRs at 512 nm (axial) and 792 nm (longitudinal). The 2-fold increase in intensity observed for the hybrid compared with the AuNRs alone could be due to the more hydrophobic (lipid bilayer) environment surrounding the AuNRs in the hybrid. Furthermore, the colloidal and optical stability of the NIR-liposome–AuNR hybrids was also demonstrated in both dextrose and serum-containing media (Figures S3 and S4). Prior to the in vivo experiments, the cytotoxicity after 3 h and 24 h of exposure to NIR-liposomes, AuNRs alone, and NIR-liposome–AuNR hybrid vesicles were determined by MTT assay on a human cell line (SH-SY5Y) of neuronal origin (Figure S5). The results indicated no significant adverse impact on cell viability.

To investigate the imaging capacity of the newly engineered hybrid vesicles in vivo, we administered them to anesthetized mice (Figure 2). MSOT imaging of the NIR-liposome–AuNR

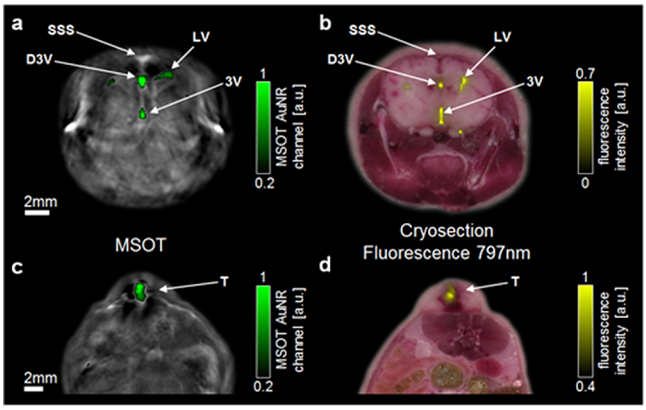

Figure 2. MSOT and fluorescence imaging of NIR-liposome–AuNR hybrids in (a, b) brain and (c, d) tumor tissue. (a) MSOT image after injection of 5 μL of the hybrid into the dorsal third ventricle (D3V) of the mouse brain. Abbreviations: SSS, superior sagital sinus; LV, lateral ventricle; 3V, third ventricle. The green overlay shows the signal detected from the AuNRs. The grayscale background is an optoacoustic image taken at 900 nm. (b) Corresponding image of cryosectioned brain tissue. The yellow overlay shows fluorescence detected from NIR-797. (c) MSOT image 6 h after direct injection of 25 μL of the hybrid into an HT29 xenograft (T). (d) Corresponding cryosection of the tumor tissue.

vesicle hybrids following intracranial (Figure 2a) and intratumoral (Figure 2c) injection in 8-week-old CD1 nu/nu female mice was performed. Signal contributions from AuNRs were imaged using MSOT and correlated with the NIR-797 fluorescence from tissue cryosections (Figure 2b,d).

To demonstrate the capability of MSOT[2,9] in spatially resolving the distribution of the injected probes deep into tissue, two distinct experiments were performed. First, the NIR-liposome–AuNR hybrids were injected into the dorsal third ventricle (D3V) of the mouse brain. The ventricles of the brain are interconnected, and therefore, the vesicles diffused throughout the ventricular cavity network of the brain following the injection. Figure 2a shows a single-wavelength (900 nm) optoacoustic image of the brain with a green overlay of the

dx.doi.org/10.1021/ja304499q | J. Am. Chem. Soc. 2012, 134, 13256–13258

multispectrally resolved optoacoustic signal from the hybrid system contributed by the AuNRs. Notably, this was achieved in deep brain matter through an intact skin and skull. Figure 2b shows the equivalent ex vivo tissue cryosection from the same animal with a yellow overlay of the fluorescent signal from the hybrids contributed by the NIR-797-labeled liposomes. In both images, the signal from the hybrids can be seen in the D3V (the site of injection) and also the lateral ventricles (LVs).

In a second experiment, intratumoral injection of the vesicle hybrids using HT29 tumor xenograft-bearing animals was performed. In Figure 2c, the signal from the hybrids was still detectable inside the tumor 6 h after injection (green overlay). Interestingly, the MSOT signal intensity in the tumor remained stable compared to 1 h after injection (Figure S6), suggesting the in vivo stability and tissue retention of the construct. Figure 2d shows the corresponding fluorescence image from the cryosectioned tumor tissue depicting the macroscopic spatial distribution of the fluorescently labeled (NIR-797) liposomes (yellow overlay). At the microscopic level, the presence of AuNRs within the tumor tissue section was further independently confirmed by dark-field microscopy (Figure S7).

The acquired MSOT data showed high resolution and contrast for deep tissue imaging in both brain and tumor in vivo. Furthermore, there was an excellent correlation between the MSOT signal (from the AuNRs) and the ex vivo epifluorescence signal of the tissue sections (from the NIR-liposomes) in both experiments. The colocalization of the AuNRs and the fluorescently labeled liposomes observed in the tissues indicates the robust structural stability of these hybrids in vivo following local administration. Most importantly, our experimental results illustrate that the AuNR-containing vesicle hybrids can act as appropriate and sensitive probes for MSOT imaging, enabling the resolution of signals from within deep-seated intact brain and tumor tissue in live animals.

In this study, previously unreported dual-labeled NIR-liposome–AuNR hybrids have been successfully engineered by self-assembly, leading to vesicular systems with high structural and colloidal stability and excellent multispectral optical properties that offer the potential to be further developed for in vivo multimodal imaging or theranostic applications. MSOT was used to illustrate the in vivo capability to visualize such hybrid vesicles within deep tissue with high-resolution imaging techniques. Moreover, the multispectral nature of MSOT not only allows the specific separation of exogenous contrast from intrinsic tissue absorbers but can also be used to resolve multiple agents of interest, such as the encapsulated contents of vesicles. One can envision further development of advanced nanoscale probes custom-designed for powerful imaging modalities (such as MSOT) based on liposome–AuNR hybrid vesicles with the inclusion of a therapeutic agent for the purposes of combinatory imaging and therapeutic applications.[10] This work shows that nanoscale systems that can be engineered to allow simultaneous visualization and transport of therapeutic agents combined with high-resolution optical imaging modalities such as MSOT hold great potential for future clinical applications.[11]

■ ASSOCIATED CONTENT

Supporting Information

Experimental section, vesicle column fractionation studies, structural characterization of preformed liposomes mixed with AuNRs, colloidal and optical stability studies in dextrose and serum-containing media, cell viability, in vivo early time (1 h) MSOT imaging within tumor tissue, and dark-field microscopy in the tumor. This material is available free of charge via the Internet at http://pubs.acs.org.

■ AUTHOR INFORMATION

Corresponding Author

v.ntziachristos@helmholtz-muenchen.de; k.kostarelos@ucl.ac.uk

Notes

The authors declare no competing financial interest.

■ ACKNOWLEDGMENTS

This work was partially supported by the Andalusian Initiative for Advanced Therapies promoted by the Regional Government of Andalusia, Spain (to N.L.). We are grateful to David McCarthy at UCL School of Pharmacy for assistance with the TEM instrumentation. V.N. acknowledges support from the ERC Advanced Investigator Award and the German Ministry of Education (BMBF) Innovation in Medicine Award.

■ REFERENCES

(1) Al-Jamal, W. T.; Kostarelos, K. *Acc. Chem. Res.* **2011**, *44*, 1094–1104.
(2) Ntziachristos, V.; Razansky, D. *Chem. Rev.* **2010**, *110*, 2783–2794.
(3) Podesta, J. E.; Kostarelos, K. *Methods Enzymol.* **2009**, *464*, 343–354.
(4) Jelveh, S.; Chithrani, D. B. *Cancers* **2011**, *3*, 1081–1110.
(5) Wang, L.; Liu, Y.; Li, W.; Jiang, X.; Ji, Y.; Wu, X.; Xu, L.; Qiu, Y.; Zhao, K.; Wei, T.; Li, Y.; Zhao, Y.; Chen, C. *Nano Lett.* **2011**, *11*, 772–780.
(6) Karg, M.; Pastoriza-Santos, I.; Perez-Juste, J.; Hellweg, T.; Liz-Marzan, L. M. *Small* **2007**, *3*, 1222–1229.
(7) Kuo, T. R.; Hovhannisyan, V. A.; Chao, Y. C.; Chao, S. L.; Chiang, S. J.; Lin, S. J.; Dong, C. Y.; Chen, C. C. *J. Am. Chem. Soc.* **2010**, *132*, 14163–14171.
(8) Wang, C.; Chen, Y.; Wang, T.; Ma, A.; Su, Z. *Adv. Funct. Mater.* **2008**, *18*, 355–361.
(9) Buehler, A.; Herzog, E.; Razansky, D.; Ntziachristos, V. *Opt. Lett.* **2010**, *35*, 2475–2477.
(10) Agarwal, A.; Mackey, M. A.; El-Sayed, M. A.; Bellamkonda, R. V. *ACS Nano* **2011**, *5*, 4919–4926.
(11) Dam, G. M.; Themelis, G.; Crane, L. M. A.; Harlaar, N. J.; Pleijhuis, R. G.; Kelder, W.; Sarantopoulos, A.; Jong, J. S.; Arts, H. J.; Zee, A. G.; Bart, J.; Low, P. S.; Ntziachristos, V. *Nat. Med.* **2011**, *17*, 1315–1320.